Microelectronics Reliability 137 (2022) 114784

Contents lists available at ScienceDirect

Microelectronics Reliability

journal homepage: www.elsevier.com/locate/microrel

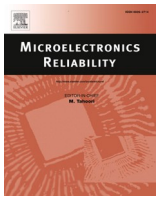

Charge deposition analysis of heavy-ion-induced single-event burnout in low-voltage power VDMOSFET

Saulo G. Alberton [a,*], V.A.P. Aguiar [a], N.H. Medina [a], N. Added [a], E.L.A. Macchione [a], R. Menegasso [a], G.J. Cesário [a], H.C. Santos [a], V.B. Scarduelli [a], J.A. Alcántara-Núñez [a], M.A. Guazzelli [b], R.B.B. Santos [b], D. Flechas [c]

[a] Instituto de Física, Universidade de Sao Paulo, São Paulo, Brazil
[b] Centro Universitário FEI, São Bernardo do Campo, Brazil
[c] Departamento de Física, Universidad Nacional de Colombia, Bogotá D.C., Colombia

ARTICLE INFO

Keywords:
Single-event burnout
Power MOSFET
Heavy-ion
Charge deposition
Worst-case

ABSTRACT

The heavy-ion-induced single-event burnout (SEB) risk in power MOSFETs (metal-oxide-semiconductor field-effect transistors) can be assessed in ground facilities, although it is costly and time-demanding. For this reason, there have been few experimental studies dedicated to investigate the relevant parameter related to the description of ion-induced SEB phenomenon. In this work the heavy-ion-induced SEB in a low-voltage power VDMOSFET (vertical double-diffused MOSFET) is studied using several ion-energy combinations. A self-consistent statistical analysis is carried out in order to elucidate the relationship between charge deposition and SEB triggering. Experimental data is compared to a predictive model from the literature for SEE (single-event effect) worst-case prediction in power MOSFETs, supporting for the first time its relevance to the worst-case prediction in the SEB mechanism.

1. Introduction

Semiconductor devices operating in harsh radiation environments may have their performance compromised, exhibiting operational failures, or even have their physical structure damaged depending on the effect caused by incident radiation. These radiation effects in semiconductor devices are called single-event effects (SEEs) when they are caused by a single ionizing particle strike. It is known that power MOSFETs exposed to a severe radiation environment typically exhibit destructive SEE such as single-event gate rupture (SEGR) and single-event burnout (SEB) [1]. Power MOSFETs are widely used in embedded systems for space applications and their susceptibility to SEEs potentially caused by the space radiation field, such as galactic cosmic rays, is typically assessed in ground facilities hosting particle accelerators [2].

Heavy-ion-induced SEB in power MOSFETs is a complex phenomenon commonly divided into three steps [3]: (I). a heavy charged particle penetrates the device under test (DUT) with enough energy to generate electron-hole pairs along its ionization track; (II). the charge carriers are multiplied in the depletion region by impact ionization, leading to a parasitic bipolar junction transistor (BJT) activation; (III) if the parasitic BJT activation is not interrupted, a second breakdown occurs and the regenerative current increase can destroy the DUT. It is known that the robustness of DMOSFETs to heavy-ion-induced SEB can be improved through some process and design techniques [4,5]. Although SEBs are destructive effects, indirect and non-destructive measurements of SEBs can be performed using a current limiting technique [6,7].

A problem that arises in the complete characterization of power MOSFETs with heavy-ion beams is related to the definition of the most adequate SEB triggering parameter. The linear energy transfer (LET) is the metric conventionally adopted for SEE characterization with heavy-ion beams [8]. However, the adoption of deposited charge or the averaged LET in the epitaxial layer is preferable for improving the characterization of power MOSFETs [2]. The most relevant parameter for the SEB triggering description has been investigated [9–12]. Using heavy-ion beams, Liu *et al.* concluded that the SEB threshold failure voltages in power MOSFETs have a better correlation, in increasing order, with the quantities: surface LET, ionized charge in the epitaxial region, and atomic number [10]. In their work, it was argued that the strong correlation with the ion atomic number Z comes from the fact that the

* Corresponding author.
E-mail address: alberton@if.usp.br (S.G. Alberton).

https://doi.org/10.1016/j.microrel.2022.114784
Received 13 June 2022; Received in revised form 26 August 2022; Accepted 7 September 2022
Available online 21 September 2022

stopping power is dependent on Z^2 in a first approximation [10]. Stassinopoulous *et al.* [11] and, more recently, Marec *et al.* [12] showed that heavy-ion-induced SEB experimental results could be better explained in terms of the accumulated charge in silicon up to the epitaxial-substrate junction.

Based on the charge deposition approach, Titus *et al.* presented a methodology for the SEE worst-case response prediction in power MOSFETs [13]. Using computational routines to calculate the heavy-ion energy deposition within the maximum epitaxial layer width, the methodology developed by these authors was successfully applied to describe the SEGR worst-case response. Titus *et al.* also emphasized the possible relevance of their model for the SEB worst-case response prediction [13], but there is still no documented experimental validation.

In this work, the heavy-ion-induced SEB phenomenon in a low-voltage power MOSFET is experimentally studied with several ion-energy combinations and a comprehensive data analysis is carried out. The charge deposition at distinct depths/layers of the DUT structure is evaluated in order to clarify which sensitive domain is related to the relevant metric for SEB triggering description. Several attempts were considered for the critical parameter p_{crit} related to SEB triggering, namely: the deposited charge within the p^+ region, the deposited charge within the depletion region, the accumulated charge in silicon up to the depletion region, the deposited charge within the epitaxial region, and the total deposited charge in silicon. In addition, the heavy-ion-induced SEB worst-case response is investigated by comparing the SEE worst-case prediction proposed by Titus *et al.* [13] with experimental data.

2. Materials and methods

2.1. SEB electrical measurements

Non-destructive SEB measurements were performed using the current limiting method [6,7]. In this method, a protection resistor R_P is responsible for limiting the electric current provided by the power supply V_{DD}, resulting in a voltage drop sufficient to reduce the DUT operational voltage necessary to trigger a second breakdown [14]. Appropriate values of R_P can be estimated if quasi-stationary avalanche curves are available [15]. As these curves are not often available to the experimentalists, R_P values of 1–10 kΩ are commonly used to protect a wide range of DUTs, in which higher resistances are preferable to protect high voltage devices [14]. An RCR network is commonly used in the gate terminal to prevent electrical stress on the DUT gate oxide [9]. The test circuitry used to perform the electrical measurements was based on [16] and it is shown in Fig. 1.

When a SEE is triggered, the DUT is temporarily switched to the ON state. In the experimental setup presented in Fig. 1, the capacitor $C_1 = 1$ nF discharges across the 50 Ω coupled resistance between the resistive logarithmic attenuator (−20 dB) and the oscilloscope (input impedance of 50 Ω) during a SEE. As discussed by Fischer [7], whether the ratio C_1/C_{OSS} is sufficiently small, where C_{OSS} is the output capacitance of the DUT, then only non-destructive SEBs are induced. The protection resistor $R_P = 1$ kΩ acts limiting the electric current provided by the power supply V_{DD} and reducing the voltage V_{DS} applied to the DUT during a high electric transient event, such as a SEB [14]. In order to avoid gate transients faster than practical switching times in MOSFETs, $R_1 = R_2 = 270$ Ω and $C_2 = 1$ nF were adopted.

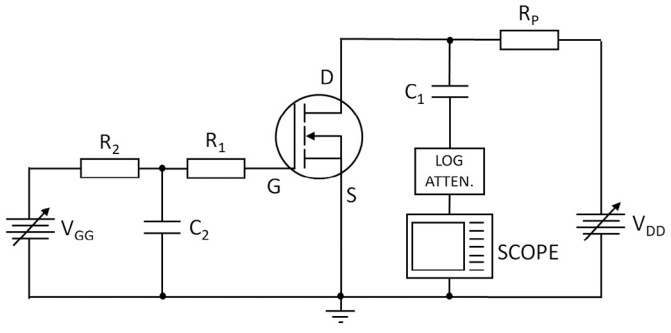

Fig. 1. Schematic circuit diagram for SET and SEB non-destructive measurements. Based on [16].

2.2. Tested device: IRLZ34NPbF

The studied DUT is a commercial *n*-type power MOSFET IRLZ34NPbF [17], with a rated breakdown voltage of 55 V. It was experimentally observed that a large increase in the drain-source leakage current i_{DSS} initiates for drain-source voltage above $V_{DS} = 73.8$ V. For this reason, the DUT breakdown voltage was estimated at about $BV_{DS} \cong 75$ V. The DUT encapsulation was removed by chemical etching to completely expose the chip surface for irradiation.

Previous studies of this device provided additional information on the composition and thicknesses of the transistor upper layers [18]. In this work, it is assumed that upper layers are composed of an aluminum (Al) metallization layer width of 0.9 μm and a SiO_2 passivation layer width of 0.9 μm. Based on [19], the p^+-base region width is estimated at $w_{p^+} = 5.0$ μm. Whether the DUT breakdown voltage is known, the epitaxial region donor concentration N_d and, then, the depletion region width w_d can be estimated according to [20]:

$$N_d = \left[\frac{5.34 \times 10^{13}}{BV_{DS}}\right]^{4/3} \quad (1)$$

$$w_d = \left[\frac{2\,\varepsilon_{Si}\,V_{DS}}{q\,N_d}\right]^{1/2}, \quad (2)$$

in which BV_{DS} is the breakdown voltage, $\varepsilon_{Si} = 1.05 \times 10^{-12}$ F/cm is the silicon permittivity and $q = 1.602 \times 10^{-19}$ C is the electron charge. The maximum depletion region width $w_{d_{max}}$ can be estimated adopting $V_{DS} = BV_{DS}$ in Eq. (2) and the epitaxial layer width is assumed to be $w_{epi} = w_{p^+} + w_{d_{max}}$. In Fig. 2 the LET curves on the DUT as a function of the heavy-ion penetration are shown. The LET values were calculated using the SRIM (Stopping and Range of Ions in Matter) code [21].

2.3. Irradiation facility

The irradiation tests were performed by combining the heavy-ion beam provided by the Sao Paulo Pelletron accelerator [22] and SAFIIRA, a dedicated beamline for radiation effects studies [23], both installed at the Nuclear Physics Open Laboratory of the University of Sao Paulo (LAFN-USP). The Sao Paulo Pelletron accelerator is an 8 MV Tandem Van de Graaff with a multi-cathode source of negative ions by Cesium sputtering (MC-SNICS), and two magnets for beam mass and precision energy selection [22]. SAFIIRA combines quadrupole defocusing and multiple scattering in two thin foils of ^{197}Au to achieve appropriate beam characteristics for radiation effects studies [23]. As a consequence of the multiple scattering, the heavy-ion beam suffers some energy degradation in comparison with its incident energy into the SAFIIRA beamline. In Table 1, the main characteristics of the heavy-ion beams used in this experiment are shown. The initial energy E_i corresponds to the beam energy provided by the Sao Paulo Pelletron accelerator. The final beam energy E corresponds to the incident beam energy on the DUT, after the energy loss due to multiple scattering in the two gold foils. The ion range (R) and the surface LET in silicon (LET_{surf}) were obtained considering the energy loss in the metallization and passivation layers of the power MOSFET.

The combination of the Sao Paulo Pelletron accelerator and SAFIIRA promotes the proper delivery of high purity ion beams with low flux, relatively low energy straggling, and high coverage area and uniformity [23]. Despite the constraint on the production of high-energy beams in such apparatus, low-energy ion beams are necessary for SEB triggering

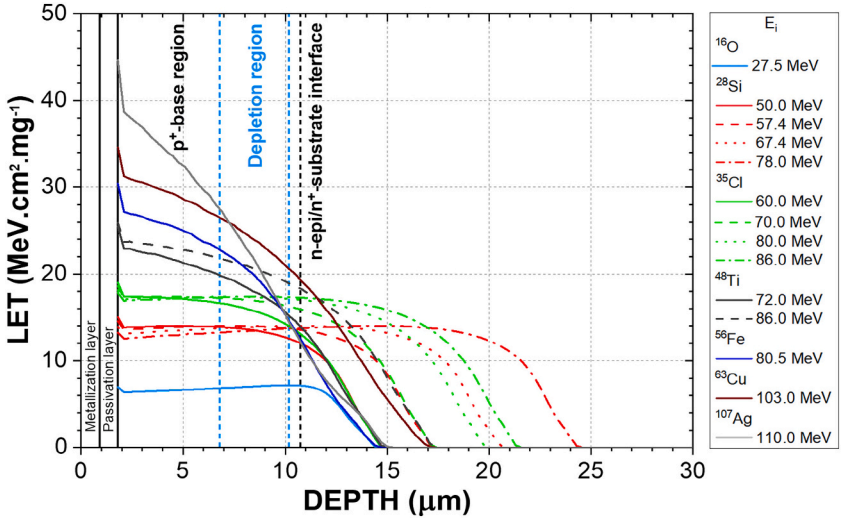

Fig. 2. Local LET along the heavy-ion penetration calculated using SRIM [21]. The discontinuity observed at the beginning of the LET curves in silicon occurs due to the SiO_2-Si transition interface. The depletion region shown here was calculated at the rated breakdown voltage.

Table 1
Heavy-ion beam characteristics for SEB experiment.

Beam	E_i (MeV)	E^a (MeV)	R^b (μm)	$LET_{surf}{}^c$ (MeV·cm²·mg⁻¹)
^{16}O	27.5	20.74 (13)	13.9 (3)	6.4
^{28}Si	50.0	41.16 (15)	14.2 (3)	13.9
	57.4	48.71 (15)	16.7 (3)	13.6
	67.4	58.9 (3)	20.1 (3)	13.1
	78.0	69.82 (15)	23.8 (3)	12.6
^{35}Cl	60.0	48.69 (19)	14.1 (3)	17.4
	70.0	58.76 (22)	16.7 (4)	17.3
	80.0	68.9 (4)	19.2 (3)	17.1
	86.0	74.96 (17)	20.8 (4)	16.9
^{48}Ti	72.0	59.0 (3)	14.2 (3)	22.9
	86.0	72.72 (21)	16.7 (4)	23.7
^{56}Fe	80.5	65.0 (7)	13.8 (5)	27.2
^{63}Cu	103.0	85.0 (4)	16.3 (5)	31.3
^{107}Ag	110.0	86.2 (16)	14.0 (7)	38.7

The final ion beam energy (E), ion range (R) and surface LET in silicon (LET_{surf}) were obtained using SRIM [19].

[a] The final beam energy uncertainty was obtained through the data of transmitted ions through two ^{197}Au thin foils.

[b] The effective range uncertainty was considered equal to the longitudinal straggling.

[c] The LET uncertainty is assumed to be 10 %, according to SRIM [21].

and worst-case studies in low-voltage power DMOSFETs, in which their sensitive domain width is estimated to be a few micrometers [13].

2.4. Test methodology

The studied power MOSFET was positioned in the irradiation chamber for frontside irradiations. The irradiation tests were carried out for several ion-energy combinations (see Table 1) in a high vacuum environment (~2×10^{-6} Torr). The typical fluence of each SEE measurement was ~10^6 particles·cm^{-2} and, whenever experimentally possible, a standard average flux of ~10^3 particles·s^{-1}·cm^{-2} was adopted. During the experiment, the DUT was maintained in the OFF-state, *i.e.*, $V_{GS} = 0$ V and $V_{DS} > 0$ V. Starting from a predefined V_{DS} value, the device was irradiated until the desired number of SEE counts was reached. The eventual electrical signals generated during an ion impact were attenuated at −20 dB with a coaxial step attenuator (Agilent 355D VHF, 1 GHz) and their waveforms were acquired by a digital oscilloscope (Rohde & Schwarz RTE 1104, 5 GSa/s, 1 GHz). The trigger levels were set at −500 mV for SEBs and −2 mV for SETs. Then, SEE cross-sections were calculated as the number of recorded events per unit fluence. At the end of a test run for the previously established V_{DS}, the V_{DS} value was increased and a new run was performed until the rated breakdown voltage of 55 V was reached. This sequential procedure was repeated for each ion-energy combination shown in Table 1.

3. Results

For low voltage power devices, both heavy-ion-induced single-event transients (SETs) and SEBs are expected to occur [24]. Sudden changes from the preset OFF-state to a temporary ON-state were verified during the irradiation tests with heavy-ion beams. Two distinct classes of waveforms induced by the heavy-ion impact were observed, differing mainly in the voltage amplitude. Low amplitude signals (~mV) were assigned as SETs, whereas high amplitude signals (~V) were assigned as SEB candidates (see Fig. 3). No heavy-ion-induced events were observed in tests with the ^{16}O heavy-ion beam. As shown in Fig. 2, the LET values for the ^{16}O beam along its path are the lowest considering all heavy-ion beams.

The cross-section of SEB candidate events was evaluated for several ion-energy combinations available at LAFN-USP (see Table 1). Few SEB events were detected with ^{28}Si ion beam at $E_i = 50.0$ MeV, even at the

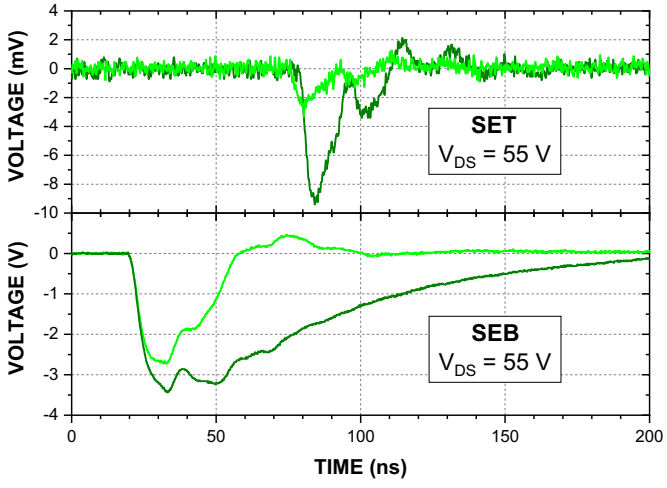

Fig. 3. Transient (top) and burnout candidate (bottom) signals recorded on the oscilloscope for ^{35}Cl beam at $E_i = 70.0$ MeV.

rated breakdown voltage of the power MOSFET. In Fig. 4, the SEB cross-sections are shown. Qualitatively, it is observed that as lower the SEB threshold failure voltage V_{DSth} is, as higher the SEB cross-sections at the rated breakdown voltage σ_{BV} are. A notable exception is the ^{63}Cu case, the last measurement series carried out in our experiment, where the minimum V_{DSth} does not correspond to the maximum σ_{BV} observed. This behavior was initially attributed to electrical stress or even destructive failures. Ion-induced physical damage was later verified on the DUT *via* scanning electron microscopy technique.

3.1. SEB saturation cross-section estimates

It is necessary to estimate the SEB saturation cross-section of the DUT for the further development of charge deposition analysis. The SEB saturation cross-section of the DUT can be properly estimated from the experimental data using a self-consistent method, *i.e.*, considering all SEB data simultaneously. Firstly, it is assumed that the σ_{SEB} dependence on V_{DS} behaves as a cumulative Weibull distribution [25]:

$$\sigma_{SEB}(V_{DS}) = \sigma_{sat}\left[1 - e^{-\left(\frac{V_{DS}-V_{DSth}}{W}\right)^{S}}\right] \quad (3)$$

in which W and S are shape parameters, σ_{sat} is the saturation cross-section, and V_{DSth} is the SEB threshold failure voltage. It should be noted that several fit parameters σ_{sat} would be obtained if Eq. (3) is fitted to each SEB data series. In this case, these values would be fit parameters related to the SEB cross-sections at the rated breakdown voltage and not necessarily to the physical saturation cross-section. The physical saturation cross-section is a function of geometry, *i.e.*, related to the architecture of the DUT [26]. Then, the best way to estimate σ_{sat} is to simultaneously fit Eq. (3) to all data sets with a globally shared saturation cross-section parameter. Good data fit quality is obtained if the ^{63}Cu data series is not considered in the global fit.

In Fig. 5 the global fit with the shared parameter is shown, resulting in $\sigma_{sat} = 4.3\ (3) \times 10^{-3}$ cm^2. The σ_{sat} obtained represents 11.1 (6) % of the die surface area. As recommended by E. Petersen [8], the results shown in Fig. 5 are replotted on a linear scale in Fig. 6 to emphasize the quality of the Weibull fits performed. As it can be seen comparing both Figs. 5 and 6, the log-linear scale attenuates the discrepancies between experimental data and Weibull data fit for higher V_{DS} values. Nevertheless, the global data fit is quite suitable for most data series.

3.2. SEB critical parameter

In this work, the SEB triggering criterion was studied based on a statistical analysis of the apparent saturation cross-section at the rated breakdown voltage, σ_{BV}, and the SEB threshold failure voltage, V_{DSth}. The charge deposition in several regions of the DUT was analyzed in order to elucidate the charge-sensitive domain for the SEB triggering description. Several critical parameter (p_{crit}) candidates related to SEB triggering were studied in this work: the deposited charge within the p^+ region ($Q_{w_{p+}}$), the deposited charge within the depletion region (Q_{w_d}), the accumulated charge in silicon up to the depletion region ($Q_{w_{p+}\to w_d}$), the deposited charge within the epitaxial region (Q_{epi}), and the total deposited charge in silicon (Q_{dep}). As usual, the deposited charge in silicon is calculated as:

$$Q = \frac{e}{\langle w_{Si}\rangle}\int \left.\frac{dE}{dx}\right|_{ioniz} dx \quad (4)$$

in which $e = 1.602 \times 10^{-19}$ C is the elementary charge, $\langle w_{Si}\rangle = 3.6$ eV is the average energy to produce an electron-hole pair in silicon and $dE/dx|_{ioniz}$ is the electronic stopping power. Considering those thicknesses previously described in Section 2.2, the calculations carried out of the deposited charge in several regions of the DUT by using Eq. (4) are presented in Table 2. In our approach, the proper dependence of σ_{BV} on p_{crit} was evaluated based on the quality of the Weibull fit and the reduced chi-square was the metric chosen to assess it. It is emphasized that, according to the previous section result, the saturation cross-

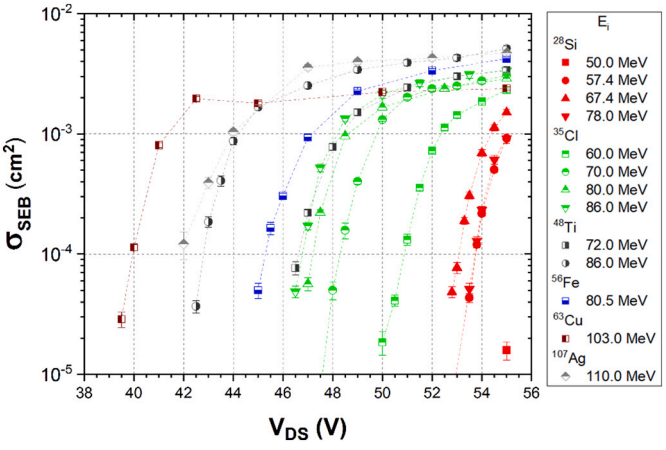

Fig. 4. SEB cross-section (σ_{SEB}) dependence on the drain-source voltage (V_{DS}) for several ion-energy combinations available with the Sao Paulo Pelletron accelerator and SAFIIRA at LAFN-USP.

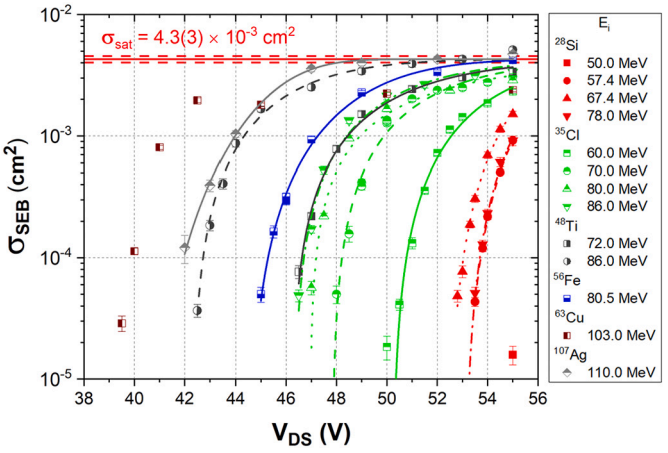

Fig. 5. SEB cross-section (σ_{SEB}) dependence on the drain-source voltage (V_{DS}) for several ion-energy combinations available at LAFN-USP. All fits were done simultaneously sharing the same saturation cross-section parameter.

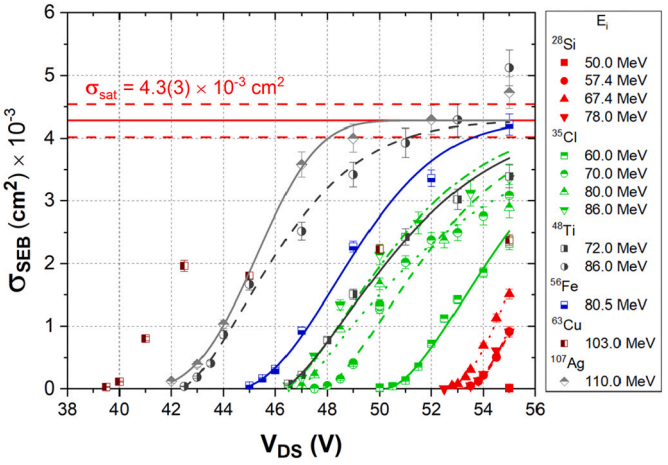

Fig. 6. Simultaneous fit with saturation cross-section as a shared parameter. It is emphasized that the data are plotted on linear scale.

Table 2
Deposited charge in several regions of the DUT.

Beam	E_i (MeV)	$Q_{w_{p+}}$ (pC)	Q_{w_d} [a] (pC)	$Q_{w_{p+}\to w_d}$ (pC)	Q_{epi} (pC)	Q_{dep} (pC)
^{28}Si	50.0	0.72	0.47	1.19	1.26	1.55
	57.4	0.71	0.48	1.20	1.28	1.90
	67.4	0.69	0.48	1.18	1.26	2.36
	78.0	0.67	0.47	1.14	1.22	2.86
^{35}Cl	60.0	0.89	0.54	1.43	1.51	1.81
	70.0	0.90	0.59	1.48	1.58	2.26
	80.0	0.89	0.60	1.49	1.59	2.72
	86.0	0.89	0.60	1.49	1.59	2.99
^{48}Ti	72.0	1.12	0.62	1.75	1.83	2.13
	86.0	1.19	0.71	1.90	2.01	2.73
^{56}Fe	80.5	1.32	0.68	1.99	2.07	2.29
^{63}Cu	103.0	1.51	0.83	2.34	2.46	3.08
^{107}Ag	110.0	1.75	0.75	2.49	2.57	2.83

The deposited charge in the p^+ region ($Q_{w_{p+}}$), the deposited charge within the depletion region (Q_{w_d}), the deposited charge in silicon up to the depletion region ($Q_{w_{p+}\to w_d}$), the deposited charge within the epitaxial region (Q_{epi}), and the total deposited charge in silicon (Q_{dep}) were calculated by using SRIM [21].

[a] Calculated considering $V_{DS} = 55$ V.

section parameter was fixed at $\sigma_{sat} = 4.3 \times 10^{-3}$ cm^{-2} in all data fits performed. In other words, it means that $\sigma_{BV}(p_{crit})$ tends to $\sigma_{sat} = 4.3 \times 10^{-3}$ cm^{-2} for higher values of p_{crit}. In Table 3, the reduced chi-square χ^2_{red} of data fits for each triggering parameter considered are shown. As can be inferred from the calculations presented in Table 2, the Q_{dep} criterion would lead to several misleading predictions. For example, the Q_{dep} criterion would indicate that the ^{28}Si at $E_i = 78.0$ MeV case would be a worst-case than ^{48}Ti at $E_i = 86.0$ MeV, which is experimentally verified to be false (see Fig. 5). On the one hand, it is found that Q_{dep} is not a good metric to describe the SEB triggering and, consequently, the data fit of σ_{BV} as a function of this parameter does not converge. On the other hand, Fig. 7 presents the dependence of σ_{BV} on Q_{w_d} and Q_{epi}, the parameters that result in the smaller values of χ^2_{red}. Concerning the χ^2_{red} metric presented in Table 3, the best results are obtained when $p_{crit} = Q_{w_d}$ is adopted.

In addition, one can also compare the proper dependence of V_{DSth} on p_{crit}. Similar to the analysis previously performed by Liu *et al.* [10], an allometric function (power law function) was chosen for the curve fitting. In their work, Liu *et al.* concluded that $V_{DS_{th}}$ has the best fitting with the ion atomic number Z than with the ion beam energy, ion range, surface LET, and ionized charge in the epitaxial region. In order to perform a fully self-consistent data analysis, the $V_{DS_{th}}$ values considered here were obtained from the global fit presented in the previous section. In Fig. 8, the curve fittings of $V_{DS_{th}}$ as a function of Q_{w_d}, Q_{epi}, and the ion atomic number Z are shown. Based on the χ^2_{red} metric for the quality of allometric fit, the SEB threshold failure voltage has the best fitting with Q_{w_d} and the worst with Z.

Although Q_{w_d} presents better results in the description of SEB triggering, it should be noted that the data spread remains present. A possible explanation may be related to the difficulty in accurately estimating the layer thicknesses of the DUT. For example, in this work the p^+-base width was roughly estimated and, once BV_{DS} is known, the depletion region width was estimated using the approximation Eq. (1) into the analytical expression Eq. (2). Thus, better accuracy when estimating the inner layers of the DUT could further improve the goodness of fit. It is also important to point out that other uncertainty sources not considered nor identified in our work might interfere with the goodness of fit. Nonetheless, the adoption of the deposited charge within the depletion region as a critical parameter is quite suitable for the heavy-ion-induced SEB triggering description.

Table 3
Goodness of fit of SEB cross-section at the rated breakdown voltage as a function of the SEB critical parameter.

Critical parameter p_{crit}	$Q_{w_{p+}}$ (pC)	Q_{w_d} [a] (pC)	$Q_{w_{p+}\to w_d}$ (pC)	Q_{epi} (pC)	Q_{dep} (pC)
χ^2_{red}	154	19	89	61	–[b]

[a] Deposited charge within the depletion region (Q_{w_d}) calculated considering $V_{DS} = 55$ V.

[b] Data fit does not converge.

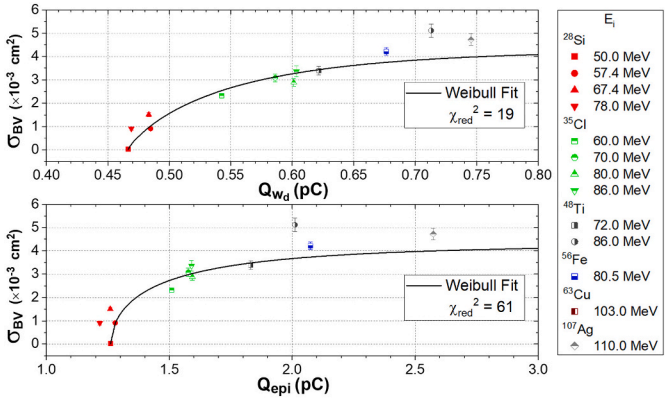

Fig. 7. SEB cross-section at the rated breakdown voltage (σ_{BV}) as a function of the deposited charge within the depletion region (top), and deposited charge within the epitaxial region (bottom). The deposited charge within the depletion region (Q_{w_d}) was calculated considering $V_{DS} = 55$ V. It is emphasized that the data are plotted on linear scale.

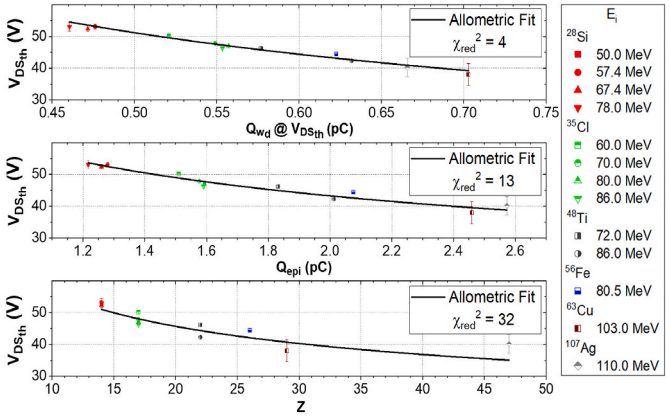

Fig. 8. SEB threshold failure voltage ($V_{DS_{th}}$) as a function of the deposited charge within the depletion region (top), the deposited charge within the epitaxial region (middle), and the ion atomic number (bottom). The deposited charge within the depletion region (Q_{w_d}) was calculated at the corresponding $V_{DS_{th}}$ for each data.

3.3. SEB worst-case: charge deposition

In Fig. 5, especially considering the ^{28}Si, ^{35}Cl, and ^{48}Ti data series, one can clearly observe the energy dependence of the SEB threshold failure voltage. The ^{35}Cl and ^{48}Ti data series present similar behavior to each other, in which increasing ion energy results in lower $V_{DS_{th}}$. On the other hand, ^{28}Si data indicate that increasing particle beam energy does not necessarily imply a lower $V_{DS_{th}}$. For example, the experimental values of σ_{SEB} for ^{28}Si at $E_i = 57.4$ MeV and $E_i = 78.0$ MeV are statistically equivalent to each other, whereas ^{28}Si at $E_i = 67.4$ MeV reveals itself as a worst test condition, relatively. Fig. 9 summarizes this result and presents the SEB cross-section contour profile of ^{28}Si data as a function of the ion energy and the supply voltage.

Based on the energy deposition approach, Titus *et al.* performed computational simulations in order to predict the SEE worst-case response in power MOSFETs [13]. In their approach, for simplicity,

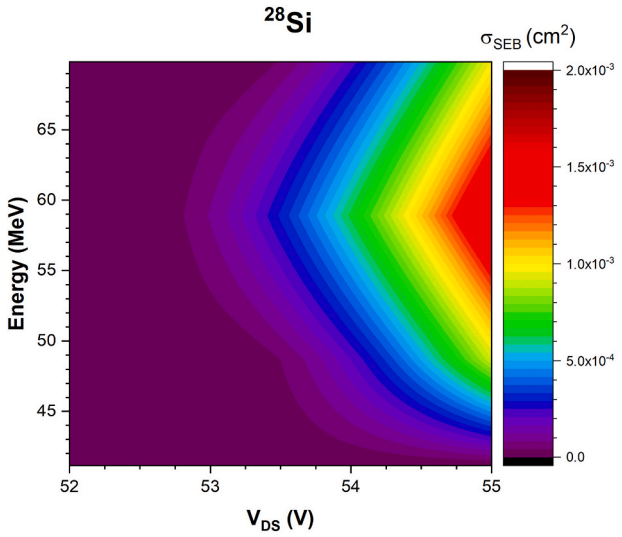

Fig. 9. SEB cross-section contour profile of ^{28}Si data as a function of ion energy and supply voltage. Colormap interpolation obtained using the global fit parameters presented in Fig. 5. (For interpretation of the references to color in this figure legend, the reader is referred to the web version of this article.)

the authors assumed that the top covering layers of the DUT were equivalent to 7 μm of silicon and the p-body thickness was equivalent to 2 μm [13]. Using the SRIM code [21] to calculate the maximum deposited energy in the DUT's epitaxial region, Titus *et al.* obtained a general-purpose analytical expression for the SEE worst-case ion energy of a DUT without a transition layer [13]:

$$E_{crit} = \left[\frac{Z^{1.333}\cdot BV_{DS}}{176} + \frac{382\cdot Z}{112 - Z}\right]\sqrt{\frac{V_{DS}}{BV_{DS}}}, \quad (5)$$

in which Z is the incident ion atomic number, V_{DS} is the drain-source applied voltage, and BV_{DS} is the breakdown voltage. The factor $\sqrt{V_{DS}/BV_{DS}}$ was later introduced to represent the depletion region modulation with respect to the applied voltage [13]. The model of Titus *et al.* was successfully applied to describe the SEGR worst-case response, but so far this model has not been tested for SEB worst-case response. In order to elucidate whether this methodology is relevant for the description of the SEB mechanism, the experimental results presented in this work are compared to Eq. (5).

The experimental results shown in Figs. 5 and 6 indicate that the SEB worst-case ion energy for ^{28}Si ($Z = 14$) is $E = 58.9$ (3) MeV (corresponding to $E_i = 67.4$ MeV, according Table 1). In the ^{28}Si data series, an inflection of the SEB cross-section as a function of the beam energy is verified (see Fig. 9). Similar behavior is not explicitly observed in the ^{35}Cl data series due to limitations in the maximum beam energy available in the test facility. Nonetheless, one can observe a convergence of the threshold voltage with respect to the beam energy. Thus, one can consider the SEB worst-case ion energy for ^{35}Cl (Z = 17) approximately equal to $E = 74.96$ (17) MeV (corresponding to $E_i = 86.0$ MeV, according Table 1).

Considering $BV_{DS} = 75.0$ V (see Section 2.2) and $V_{DS} = 55.0$ V, Eq. (5) results in $E_{crit} = 59.0$ MeV for ^{28}Si ($Z = 14$) and $E_{crit} = 74.5$ MeV for ^{35}Cl ($Z = 17$). The comparison between Eq. (5) and the experimental results of this work is summarized in Table 4. Consequently, one can conclude that the methodology of Titus *et al.* provides good agreement with the experimental data, suggesting that it is also useful for the SEB worst-case response prediction in low-voltage power VDMOSFETs.

4. Discussion

The method of Titus *et al.* assumes that the epitaxial region of the DUT is the critical sensitive domain related to SEEs in power VDMOSFETs [13]. As it was shown in the previous section, this assumption is adequate to predict the SEB worst-case response. On the other hand, our statistical analysis has shown that the depletion layer is a better metric to describe the SEB occurrence once it is triggered. The effectiveness of the charge deposition criterion within the epitaxial region on the worst-case description can be clarified through computational simulations based on the methodology of Titus *et al.* [13]. Fig. 10 presents the charge deposition dependence on the ion energy considering the Si-equivalent model for the DUT thicknesses proposed by Titus *et al.* (covering layers and a p-body thickness equivalent to 7 μm and 2 μm of silicon, respectively) [13], and for those thicknesses adopted in this work, described in Section 2.2. In Fig. 10 one can see that the predicted critical energies are approximately equivalent to each other for both charge deposition criteria considered. Therefore, this would explain why the deposited charge in the epitaxial region is also a good metric for worst-case prediction although it has not proved to be the most suitable parameter for the general description of the SEB triggering.

Based on the charge deposition model, a small dependence of the SEB failure voltage on the ion range/energy should be expected for high-energy projectiles whose range considerably exceeds the DUT sensitive domain. For example, when testing VDMOSFETs with relatively high energy ions, an energy increase may result in a small reduction in the amount of deposited charge on the DUT sensitive domain. This is precisely indicated in the asymptotic behavior of the charge deposition curve presented in Fig. 10.

Finally, concerning the SEB sensitive domain, the high sensitivity of the depletion region on the ion-induced SEB phenomenon in VDMOSFETs was previously predicted by two-dimensional numerical

Table 4
Critical heavy-ion energy for SEE worst-case response at 55 V.

	Experimental	Titus *et al.* prediction Eq. (5) [13]
Beam	E_{crit} (MeV)	
^{28}Si	58.9 (3)	59.0
^{35}Cl	74.96 (17)[a]	74.5

[a] Worst-case experimentally achievable (maximum energy available in the test facility).

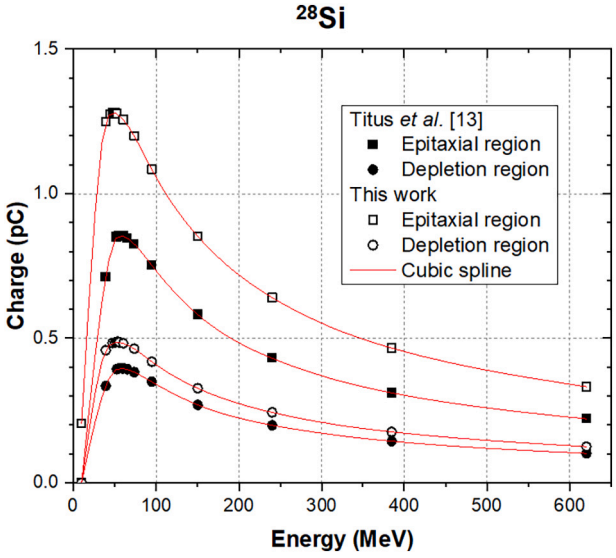

Fig. 10. Calculation of the deposited charge within distinct sensitive domains (epitaxial and depletion region at 55 V) for ^{28}Si ion beam incident on the DUT at several energies. Two models were considered for the device structure: the Si-equivalent model by Titus *et al.* [13], and the layer structure described earlier in Section 2.2 of this work.

simulations [27,28]. These computational results are supported by the experimental data and statistical analysis presented in this work.

5. Conclusion

This work presents a comprehensive data analysis of heavy-ion-induced SEB in a low-voltage power VDMOSFET. Statistical analysis of the SEB cross-section and threshold failure voltage data suggests that the deposited charge within the depletion region is the relevant metric for the description of SEB triggering. Best fittings were obtained when considering this quantity as the SEB critical parameter. A good agreement was observed between the SEE worst-case response prediction of Titus *et al.* [13] and our SEB worst-case experimental data. This result provides first evidence that the methodology of Titus *et al.* based on charge deposition is also relevant for failure prediction in the SEB mechanism. Further work is needed to check the extent of validity of the predictive model for a wide range of breakdown voltage, as well as for other power transistor technologies.

Declaration of competing interest

The authors declare that they have no known competing financial interests or personal relationships that could have appeared to influence the work reported in this paper.

Data availability

Data will be made available on request.

Acknowledgments

The authors would like to acknowledge Prof. Dr. Wayne A. Seale for the English revision of this manuscript, the LAFN technical staff for their support, and the Brazilian Agencies CNPq (proc. no. 434609/2018-8 and 306353/2018-0) and FAPESP (proc. no. 2012/03383-5) for financial support. This work is a part of the projects CITAR (FINEP proc. no. 01.12.0224.00) and INCT-FNA (proc. no. 464898/2014-5). This study was financed in part by the Coordenação de Aperfeiçoamento de Pessoal de Nível Superior – Brasil (CAPES) – Financial Code 001.

References

[1] F.W. Sexton, Destructive single-event effects in semiconductor devices and ICs, IEEE Trans. Nucl. Sci. 50 (3) (June 2003) 603–621.
[2] V. Ferlet-Cavrois, et al., Charge collection in power MOSFETs for SEB characterisation—evidence of energy effects, IEEE Trans. Nucl. Sci. 57 (6) (Dec. 2010) 3515–3527.
[3] J.H. Hohl, K.F. Galloway, Analytical model for single event burnout of power MOSFETs, IEEE Trans. Nucl. Sci. 34 (6) (Dec. 1987) 1275–1280.
[4] T.F. Wrobel, et al., Solutions to heavy ion induced avalanche burnout in power devices, IEEE Trans. Nucl. Sci. 39 (6) (Dec. 1992) 1636–1641.
[5] S. Liu, et al., Effect of buffer layer on single-event burnout of power DMOSFETs, IEEE Trans. Nucl. Sci. 54 (6) (Dec. 2007) 2554–2560.
[6] D.L. Oberg, J.L. Wert, First nondestructive measurements of power MOSFET single event burnout cross-sections, IEEE Trans. Nucl. Sci. 34 (6) (Dec. 1987) 1736–1741.
[7] T.A. Fischer, Heavy-ion-induced, gate-rupture in power MOSFETs, IEEE Trans. Nucl. Sci. 34 (6) (Dec. 1987) 1786–1791.
[8] E. Petersen, Single Event Effects in Aerospace, John Wiley & Sons, 2011.
[9] J.L. Titus, An updated perspective of single event gate rupture and single event burnout in power MOSFETs, IEEE Trans. Nucl. Sci. 60 (3) (June 2013) 1912–1928.
[10] S. Liu, et al., Effects of ion species on SEB failure voltage of power DMOSFET, IEEE Trans. Nucl. Sci. 58 (6) (Dec. 2011) 2991–2997.
[11] E.G. Stassinopoulos, et al., Charge generation by heavy ions in power MOSFETs, burnout space predictions and dynamic SEB sensitivity, IEEE Trans. Nucl. Sci. 39 (6) (Dec. 1992) 1704–1711.
[12] R. Marec, et al., Methodology to predict the SEE rate in vertical MOSFET with deep charge collection, in: ESA/ESTEC QCA Final Presentation Days, Villigen, Switzerland, 2009. Available: https://escies.org/download/webDocumentFile?id=19716.
[13] J.L. Titus, C.F. Wheatley, SEE characterization of vertical DMOSFETs: an updated test protocol, IEEE Trans. Nucl. Sci. 50 (6) (Dec. 2003) 2341–2351.
[14] S. Liu, et al., Evaluation on protective single event burnout test method for power DMOSFETs, IEEE Trans. Nucl. Sci. 59 (4) (Aug. 2012) 1125–1129.
[15] S. Liu, et al., Single-event burnout and avalanche characteristics of power DMOSFETs, IEEE Trans. Nucl. Sci. 53 (6) (Dec. 2006) 3379–3385.
[16] F. Miller, et al., Characterization of single-event burnout in power MOSFET using backside laser testing, IEEE Trans. Nucl. Sci. 53 (6) (Dec. 2006) 3145–3152.
[17] International Rectifier, "HEXFET® Power MOSFET," IRLZ34NPbF Datasheet, Nov. 2003.
[18] M.B. Paschoal, Efeitos da radiação ionizante provenientes de raios-X e feixe de prótons nas propriedades de semicondutores, Centro Universitário FEI, Brazil, 2017. http://sofia.fei.edu.br:8080/pergamumweb/vinculos/00002c/00002cd7.pdf. (Accessed 7 May 2021) (B.S. Thesis, Online).
[19] A.E. Waskiewicz, J.W. Groninger, Burnout Thresholds and Cross-section of Power MOS Transistors With Heavy Ions. Technical Report, Rockwell International Corporation, 1990.
[20] B.J. Baliga, Fundamentals of Power Semiconductor Devices, Springer Science & Business Media, 2010.
[21] SRIM—the Stopping and Range of Ions in Matter, Available: http://www.srim.org/ (Online).
[22] O. Sala, G. Spalek, The nuclear structure facility at the University of São Paulo, Nucl. Inst. Methods 122 (1974) 213–225.
[23] V.A.P. Aguiar, et al., SAFIIRA: a heavy-ion multi-purpose irradiation facility in Brazil, Rev. Sci. Instrum. 91 (May 2020), 053301.
[24] F. Velardi, et al., Experimental study of charge generation mechanisms in power MOSFETs due to energetic particle impact, Microelectron. Reliab. 43 (2003) 549–555.
[25] N.J. McCormick, Reliability and Risk Analysis: Methods and Nuclear Power Applications, Academic Press, 1981.
[26] E.L. Petersen, Single-event data analysis, IEEE Trans. Nucl. Sci. 55 (6) (Dec. 2008) 2819–2841.
[27] A. Luu, et al., Sensitive volume and triggering criteria of SEB in classic planar VDMOS, IEEE Trans. Nucl. Sci. 57 (4) (Aug. 2010) 1900–1907.
[28] M. Zerarka, et al., Behavioral study of single-event burnout in power devices for natural radiation environment applications, IEEE Trans. Electron Devices 59 (12) (Dec. 2012) 3482–3488.